A methodology for attributing extratropical cyclones to climate change: the case study of storm Alex 2020

Mireia Ginesta, Pascal Yiou, Gabriele Messori, Davide Faranda

A methodology for attributing severe extratropical cyclones to climate change based on reanalysis data: the case study of storm Alex 2020

Mireia Ginesta[1*], Pascal Yiou[1], Gabriele Messori[2,3] and Davide Faranda[1,4,5]

[1*]Laboratoire des Sciences du Climat et de l'Environnement, LSCE/IPSL, CEA-CNRS-UVSQ, Université Paris-Saclay, Gif-sur-Yvette, 91191, France.
[2]Department of Earth Sciences and Centre of Natural Hazards and Disaster Science (CNDS), Uppsala University, Uppsala, Sweden.
[3]Department of Meteorology and Bolin Centre for Climate Research, Stockholm University, Stockholm, Sweden.
[4]London Mathematical Laboratory, 8 Margravine Gardens London, W6 8RH, London, United Kingdom.
[5]LMD/IPSL, Ecole Normale Superieure, PSL research University, Paris, France.

*Corresponding author(s). E-mail(s): Mireia.Ginesta-Fernandez@lsce.ipsl.fr;
Contributing authors: pascal.yiou@lsce.ipsl.fr; gabriele.messori@geo.uu.se; davide.faranda@lsce.ipsl.fr;

Abstract

Extreme event attribution aims at evaluating the impact of climate change on specific extreme events. In this work, we present an attribution methodology for severe extratropical cyclones, and test it on storm Alex. Alex was an explosive extratropical cyclone that affected Southern France and Northern Italy at the beginning of October 2020. The methodology exploits mathematical properties of circulation analogues, and identifies changes in physical and statistical properties. We first

divide 6-hourly ERA5 data into two periods: a counterfactual period (1950–1984) and a factual period (1986–2021). We then identify the 30 cyclones in each period whose sea-level pressure maps are closest to Alex's map by selecting those with the lowest Euclidean distance from Alex. We term these "analogues" of Alex. We find that analogues in the factual period are more persistent than in the counterfactual period, which may favour severe impacts resulting from persistent strong winds and heavy precipitation, as was the case for Alex. This effect is compounded by the doubling in accumulated daily precipitation detected in Northern Italy between the counterfactual and factual analogues. In the factual period, the analogues display an increase in the eddy kinetic energy in their growth phase, with poleward-shifted backward tracks. We also identify a seasonal shift of the analogues, from spring to autumn. Finally, the analogues in the factual period are closer to Alex than in the counterfactual period. These changes collectively point to high-impact storms like Alex having become more common in a changing climate.

Keywords: Extratropical explosive cyclones, Extreme Event Attribution, Climate Change, Analogues

Acknowledgments

This work was supported by the European Union's Horizon 2020 research and innovation programme under the Marie Sklodowska-Curie grant agreement N° 956396 (European weather extremes: drivers, predictability and impacts (EDIPI) ITN). The authors wish to thank S Bourdin, J Riboldi, M Rodrigo, F Pons, S Thao and Y Robin for useful discussions, J Pinto for sharing the ERA5 tracks database, and two anonymous reviewers for their constructive comments.

1 Introduction

Under global warming, the atmosphere is experiencing dynamic and thermodynamic changes (Allan et al, 2021). Understanding and predicting such changes is an essential step in order to evaluate climate-related hazards today and in the future (Pörtner et al, 2022). A major effort in this direction has been achieved with extreme event attribution (EEA) (National Academies of Sciences, Engineering, and Medicine, 2016). EEA is an emerging field that originated in the early 2000s (e.g. Stott et al, 2004) whose objective is to estimate to what extent climate change influences the likelihood and severity of specific extreme climate events. Extreme event attribution combines statistical analyses and physical understanding (Stott et al, 2016), and has been applied to a broad range of extremes events, including droughts, cold spells, heatwaves or extreme rainfall events (e.g. Philip et al, 2018; Cattiaux et al, 2010; Stott et al, 2004; Jézéquel et al, 2018; Pall et al, 2011).

Some extreme event categories have nonetheless proved more difficult to analyse in an attribution framework than others. An example are extratropical cyclones (ETCs), whose location, frequency and intensity depend on a combination of large-scale, synoptic-scale and smaller dynamic and thermodynamic features (Shapiro et al, 1999). This makes it challenging to both understand recent trends in ETC occurrence and project future ones (e.g. Shaw et al, 2016). In the Northern Hemisphere (NH), the number of ETCs has likely increased in recent decades (Chang and Yau, 2016), while there is evidence of a decrease in the number of NH extreme cyclones in winter (Neu et al (2013), referred to as deep cyclones) and in summer (Chang et al (2016), referred to as strong cyclones). However, there is low confidence for such changes as they are subject to high internal variability and regional variations and they are sensitive to the choice of reanalysis (Tilinina et al, 2013) and cyclone detection and tracking methods (Neu et al, 2013). In future climate projections, the number of ETCs in the storm track regions is projected to decrease globally, while the number of extreme cyclones is likely to increase in NH winter (Priestley and Catto, 2022). As stated in the last IPCC report, the precipitation associated with ETCs over the NH (Seneviratne et al, 2021) and the number of ETCs associated with extreme precipitation (Lee et al, 2021) are projected to increase (high confidence). However, there is a less clear response regarding wind speed changes, which are expected to be small and subject to regional variations (Seneviratne et al, 2021).

These global or hemispheric-scale changes mask a number of important regional trends, although in many cases it may be difficult to determine to which extent these depend on long-term climatic changes or on low-frequency internal climate variability. For example, in the North Atlantic, there is evidence of an overall poleward shift of the storm track between 1979 and 2010 (Tilinina et al, 2013). The same authors state that very deep cyclones (<960 hPa) increased in frequency in the North Atlantic region from 1979 to 1990 in most reanalyses, and declined thereafter. However, such changes may be modulated by the interdecadal variability of the North Atlantic Oscillation (Feser et al, 2015). Simulations of future climates from the Coupled Model Intercomparison Project phases 5 and 6 (CMIP5 and CMIP6) project a tripolar anomaly pattern in winter North Atlantic storm track, with an extension of storm activity further into Europe and a decrease on the storm track's northern and southern flanks (Harvey et al, 2020; Zappa et al, 2013; Priestley and Catto, 2022). CMIP5 models and Regional Climate System Models from the Med-CORDEX initiative also show a weakening of the storm activity over the Mediterranean region (Zappa et al, 2015; Reale et al, 2022). However, according to the last IPCC report (Lee et al, 2021), there is low confidence in regional change projections in the NH and especially in the North Atlantic in winter due to "large natural internal variability, the competing effects of projected upper- and lower-tropospheric temperature gradient changes, and new evidence of weaknesses in simulating past variations in North Atlantic atmospheric circulation on seasonal-to-decadal timescales".

The uncertainty surrounding past and future regional trends in ETCs highlights the difficulty in attributing their occurrence to climate change. Here, we present an attribution methodology applicable to severe extratropical cyclones, and test it on storm Alex: an explosive cyclone that affected France and Italy in October 2020. We demonstrate that a combination of analogue analysis, dynamical systems theory and extreme value theory enables to attribute the characteristics and impacts of individual extratropical cyclones to the ongoing climatic changes.

The paper is organized as follows: section 2 describes the characteristics of Alex. Section 3 provides a detailed description of the data and methods used. It is followed by the presentation of the results in section 4 and a discussion and conclusion in section 5.

2 Alex: a high-impact explosive cyclone

Storm Alex was a powerful explosive cyclone (Sanders and Gyakum, 1980; Neu et al, 2013) that affected south-western Europe in October 2020. It formed as a small perturbation south of Greenland and was named by Météo-France on the 1st of October. Favoured by a very strong jet stream with core speeds of up to 100 m/s, Alex deepened rapidly and experienced explosive cyclogenesis between the 1st and the 2nd of October with a deepening rate of 1.62 Bergeron. The cyclone made landfall in Brittany on the night between the 1st–2nd October, with very intense surface winds of up to 140 km/h that caused widespread damage. On the 2nd of October in the early morning the cyclone reached its minimum pressure with values around 970 hPa (such as 969,6hPa in Vannes, France (Météo France, 2021)). The size of the cyclone was about $2x10^6$ km^2, with an effective radius of 810 km, computed using the area enclosed in the last closed isobar with 1 hPa step using the ERA5 reanalysis dataset (Hersbach et al, 2020). Alex then remained stationary over the English channel for a day. Southeasterly winds were induced in southern France and northern Italy, carrying warm, humid air from the Mediterranean and producing extremely heavy rainfall and strong winds. This phenomenon is known as a Mediterranean episode (WMO, 2020). On the 3rd of October the cyclone weakened and moved to Normandy. Finally, on the 4th of October, Alex headed northward to England and dissipated during the following days over the North Sea. Figure 1 shows Alex's backward and forward trajectories. It also shows the maximum wind gusts over land and the total accumulated precipitation over the domain between the 1st and the 4th of October at 06:00 UTC. As a caveat, it is possible that not all the precipitation and wind gusts displayed in Figure 1 are directly associated with storm Alex.

The persistence of storm Alex over the same region resulted in severe impacts, especially in southern France and northern Italy. The area located windward of the Alps received heavy and prolonged orographically-driven rainfall, leading to numerous record-breaking precipitation amounts registered in the Alpes-Maritimes, Var and Piedmont regions. Piedmont had the highest

rainfall since 1951, recording 630 mm in 24h in Sambughetto (European State of the Climate, 2020). Saint-Martin-Vésubie, a village in Alpes-Maritimes, recorded 501 mm of precipitation in 24 hours (Météo France, 2020a), which corresponds to more than three times the climatological October precipitation (Météo France, 2020b). Alex caused at least 23 fatalities (10 in France, 10 in Italy, 1 in Austria, 1 in Poland and 1 in the Czech Republic), more than 10 missing people and an estimated economic loss of about 2.7 billion euros (Météo France, 2021; Riviera 24, 2021; The Watchers, 2020; Aon, 2020).

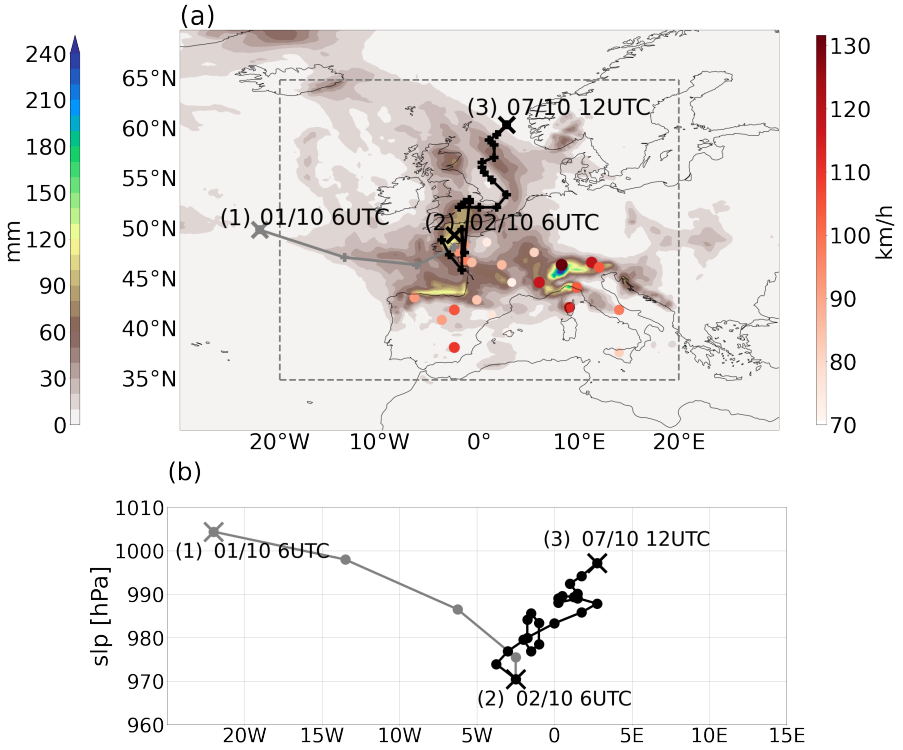

Fig. 1 (a) Backward (grey) and forward (black) trajectories of storm Alex relative to its point of maximum intensity. Total accumulated precipitation (shading) and maximum 10m wind gusts (coloured dots) between 01/10/2020 at 06:00 UTC and 04/10/2020 at 06:00 UTC, when Alex had its largest impacts. The numbers indicate when cyclogenesis occurred (1), when Alex reached its minimum sea-level pressure (2), and when it underwent cyclolysis (3). Dashed lines indicate the spatial domain used to find the analogues, covering (20W–20E, 35–65N). We use ERA5 6-hourly data to track the cyclone, and ERA5 hourly data to obtain the accumulated precipitation and maximum 10m wind gusts (see Section 3 for further details). The maximum 10m wind gusts were obtained for every region of France, Italy, and Spain, using spatial masks according to NUTS2 regions (Eurostat, 2021); here we only present some regions to have a general view of the storm's impacts. (b) The corresponding sea-level pressure evolution at the cyclone center as a function of time and longitude.

3 Methodology

We compute flow analogues (Yiou, 2014) to find pattern recurrences of Alex in mean sea-level pressure (SLP), and assess changes in the analogues within the ERA5 reanalysis dataset (Hersbach et al, 2020). We use 6-hourly data from 1950 to 2021, which we split into two 35-year periods: a factual period, from November 1986 to November 2021, and a counterfactual period, from January 1950 to December 1984. We refer to them as [1986-2021] and [1950-1984], respectively. The latter is meant to represent a climate only weakly affected by anthropogenic emissions, while the former presumably displays a stronger anthropogenic influence. This assumption is supported by a substantial change in the effective-radiative forcing from the 1980s onwards, as shown in Figure 2.10 of Chapter 2 in the last IPCC Sixth Assessment Report, (Gulev et al, 2021), and by a significant increase in the number of storms in the North Atlantic in the factual period with respect to the counterfactual (Fig. B1). The number of storms has been counted using the *TempestExtremes* software package (Ullrich et al, 2021; Ullrich and Zarzycki, 2017; Zarzycki and Ullrich, 2017). We pick 35-year periods as a balance between needing periods that are short enough to assume a relatively constant climate state, yet long enough to assume that interannual variability issued from periodic variations such as the El-Niño – Southern Oscillation averages out. Adopting two periods around 30-year long is a common practice in attribution studies (e.g. Luu et al, 2018; Vautard et al, 2019). We have tested that changing the periods slightly (e.g. [1950-1975] and [1995-2020]) do not alter qualitatively the results.

3.1 Analogue circulation patterns

We identify the 2nd of October 2020 at 6:00UTC as approximately when storm Alex reached its lowest central pressure (970.48hPa according to ERA5 data) while stalling over the English Channel. We term this time step *lag 0* date of Alex. We then use mean sea-level pressure to identify the best 30 analogue cyclones in the counterfactual and factual periods. To select the analogues, we compute the Euclidean distance between the sea-level pressure maps of the 2nd of October 2020 at 06:00UTC and all other time steps at each grid point of the spatial domain covering [20W–20E, 35–65N] (dashed-line box in Figure 1a). Then, we average the Euclidean distances for all grid boxes across the domain for each timestep, resulting in a time series of domain-averages Euclidean distances. The 30 analogues are the timesteps that display the 30 smallest Euclidean distances. To avoid counting several times the same cyclone, we impose a minimum 7-day separation between analogues. This is justified by the fact that 3 days is a typical timescale for the formation and decay of an extratropical cyclone (Moon et al, 2021), but that specific cyclones can last longer than this (e.g. Alex lasted 7 days). Since our main purpose is to find distinct storms similar to Alex in order to assess changes in their dynamical characteristics, we deem a 7-day separation appropriate. Changes in the spatial domain of up to 10 degrees do not alter the results in a significant manner.

Some quantitative changes are however expected when the domain is modified, as the analogues include information about all atmospheric structures within the chosen domain. The choice of 30 analogues is a balance between the needs to have a large enough sample size to make statistical inferences, and to have analogues that are suitably close to the reference event we are studying. Using 25 or 40 analogues rather than 30 does not change our results substantially. We have computed the average Euclidean distance of the closest 30 events for each sea-level pressure map of the two periods and found no significant differences in the probability distributions (Fig. B2). Hence, we conclude that 30 analogues is a robust choice.

Once we have obtained the *lag 0* dates of the 30 best analogues – namely the dates when the minimum Euclidean distance for each analogue is attained – we compute their composite maps for several variables of interest for each period, and the difference map between them. Figures B3 and B4 show the mean sea-level pressure patterns at the *lag 0* dates of the 30 analogues in the counterfactual and factual period, respectively. Additional variables of interest include geopotential height at 500 hPa (Z500), eddy kinetic energy at 500 hPa (EKE500), 24-hour accumulated precipitation (PR), 2m air temperature averaged over 24 hours (T2M), maximum 10m wind gust within 24 hours (WG), and deseasonalized 2m air temperature (T2Mdes). EKE500 is computed using a 24-hours difference filter (Wallace et al, 1988). WG is the maximum 3-second wind at 10 m height as defined by the World Meteorological Organization (WMO, 1987), where the gust is computed at every time step and the maximum is kept since the previous post-processing. To compute PR and WG, we use hourly data, and to evaluate T2M we use 6-hourly data. The start times to compute the accumulated values for PR, average values for T2M and maximum values for WG are the *lag 0* dates and end times are 24 hours after them, that is, at *lag +24* hours. To evaluate T2Mdes, we first compute a 31-day running-mean smoothed seasonal cycle for each period. We then subtract the smoothed seasonal cycle from the T2M data.

For each analogue, we compute 48 hours backward and forward cyclone trajectories with a 6-hours time step using a semi-objective Lagrangian approach. Cyclone centers are automatically identified by following the absolute minimum sea-level pressure. We have then checked and corrected each trajectory manually if needed, which induces some subjectiveness in our method. Some cyclones originate from secondary cyclogenesis, that is, from the trailing fronts of a 'primary cyclone' (Parker, 1998; Priestley et al, 2020). They are typically diagnosed by a trough in the sea-level pressure configuration of the primary cyclone. Here we detect them using a semi-objective method where troughs are detected visually but are required to have a minimum depth of 5hPa. We have compared factual cyclone tracks with those obtained following Pinto et al (2005), which corresponds to the method M02 from Neu et al (2013) of the Intercomparison of Mid Latitude Storm Diagnostics (IMILAST), without finding any qualitative differences. Hence, the tracking method used here is not expected to alter our results and conclusions.

We count the number of cyclones that experienced explosive cyclogenesis following the definition of Sanders and Gyakum (1980) as those with a Normalized Central Pressure Deepening Rate (NDR, Reale et al (2019)) greater than 1. We also count the number of cyclones entering the Mediterranean region as those that, after 24 hours or more, are located at latitudes south of 43°N and longitudes east of 3°E.

We finally assess the quality of analogues. We first compute *SLP anomalies* by subtracting Alex's SLP from the mean SLP of the analogues in the two periods. Second, we represent the probability distributions of the values of the SLP Euclidean distances between Alex and its analogues and we term it *analogues quality*.

3.2 Dynamical systems metrics

In order to characterise the dynamics of storm Alex and its analogues, we use local dimension and persistence metrics issued from dynamical systems theory. These metrics describe the local properties of a dynamical system (Lucarini et al, 2016), which for atmospheric data may be related to the characteristics of instantaneous regional atmospheric patterns (e.g. Messori et al, 2017; Faranda et al, 2017; Alvarez-Castro et al, 2018; Messori et al, 2021).

We follow the approach from Faranda et al (2017) and Lucarini et al (2016), who combine extreme value theory with dynamical systems theory to compute the local dimension d and persistence θ^{-1} of dynamical systems. Local dimension d describes the phase-space geometry of the trajectories in the neighbourhood of a certain state of the system. The higher d, the higher the number of possible evolutions to and from that state. The persistence θ^{-1} measures the average residence time around a given state, and is given by the inverse of the extremal index θ. θ has units of frequency (here 1/6 hours^{-1}, as we use 6-hourly data). Hence, to find the persistence in hours, we multiply θ^{-1} by a factor of 6. A detailed description of the procedure to compute d and θ^{-1} is provided in Appendix A.

3.3 Assessing statistical significance

To assess the statistical significance of the differences between the analogues' averages in the factual and counterfactual periods, we apply a bootstrap procedure with 1000 iterations (Wilks, 2005). Our null hypothesis is that both sets of analogues are drawn from distributions with the same mean. If the difference of the two original samples — factual minus counterfactual — has an absolute value larger than the 95th percentile of the bootstrap distribution, we reject the null hypothesis and conclude that the differences are statistically significant. To compute Confidence Intervals (CI) for statistical samples we again apply a bootstrap procedure with 1000 iterations, with a 95% confidence level, namely taking the 2.5th and 97.5th percentiles of the bootstrap distribution as the lower and upper bounds, respectively. To evaluate the CI of the local dimension d we resample the exceedances of the threshold $s(q)$ (see section A)

and compute d in each iteration. To calculate the CI of the extremal index θ we resample the inter-cluster and cluster sizes with equal probabilities (Süveges, 2007), and compute θ for each sampling iteration. Finally, the statistical significance of the differences between boxplots is assessed using a two-sample Kolmogorov-Smirnov test (Wilks, 2005), with a 5% significance level. The null hypothesis is that both data samples belong to the same, unknown distribution.

4 Results

4.1 Circulation patterns

Figure 2a–c shows the SLP map for the *lag 0* time step of Alex and the composite SLPs for analogues during the counterfactual and factual periods, respectively. Both sets of analogues capture the large-scale structure of Alex, albeit with a weaker magnitude as may be expected by the average of 30 events. Note that when computing the Euclidean distances to find the analogues we use the domain shown by the dashed-line box in Fig. 1, and so the North Atlantic large-scale atmospheric configuration might differ between analogues. The difference between the two analogue composites (Fig. 2d) displays an SLP dipole: high pressure anomalies over the North Atlantic and low pressure anomalies over North Africa. This northward (southward) extension of the high (low) pressure system yields an increase in the waviness of the pattern in the factual period. No significant differences are found at the cyclone center. In the middle troposphere (Z500), the analogues capture the low pressure structure over England that characterised Alex (Fig. 2e, f, g). The Z500 differences between the analogues in the two periods (Fig. 2h) partly resemble those in SLP: there is a northward extension and a strengthening of the Azores anticyclone, enhancing the waviness of the pressure field.

Fig. 3 shows Alex's SLP and Z500 and the composite SLP and Z500 of the analogues 12 hours after *lag 0* dates, that is, at *lag +12* hours. We find negative, albeit marginally significant, SLP anomalies over the cyclone core region. In the mid-troposphere, Z500 shows high-pressure anomalies over the North Atlantic. The pattern of the background flow is thus wavier in the factual period, as for *lag 0*, due to low-pressure anomalies in the cyclone region and upstream high-pressure anomalies.

We further analyse the EKE500 maps for Alex and its analogues (Figure 2i–l) 24 hours before *lag 0* dates, that is, at *lag -24h* hours. There is a clear difference between Alex's EKE500 and that of the analogues in both periods, which emphasizes that the analogue storms have different origins across the North Atlantic basin. Composite EKE500 analogue differences between the two periods (Fig. 2l) show a dipole of positive anomalies west of England and weaker negative anomalies at lower latitudes, representing a poleward shift in the factual period with respect to the counterfactual. In addition, EKE500 differences centered at 48 hours before Alex show this dipole but shifted about 10° to the west (Fig. B5). This pattern suggests a higher-latitude origin of the storms in the factual period, consistent with the increase in the waviness found

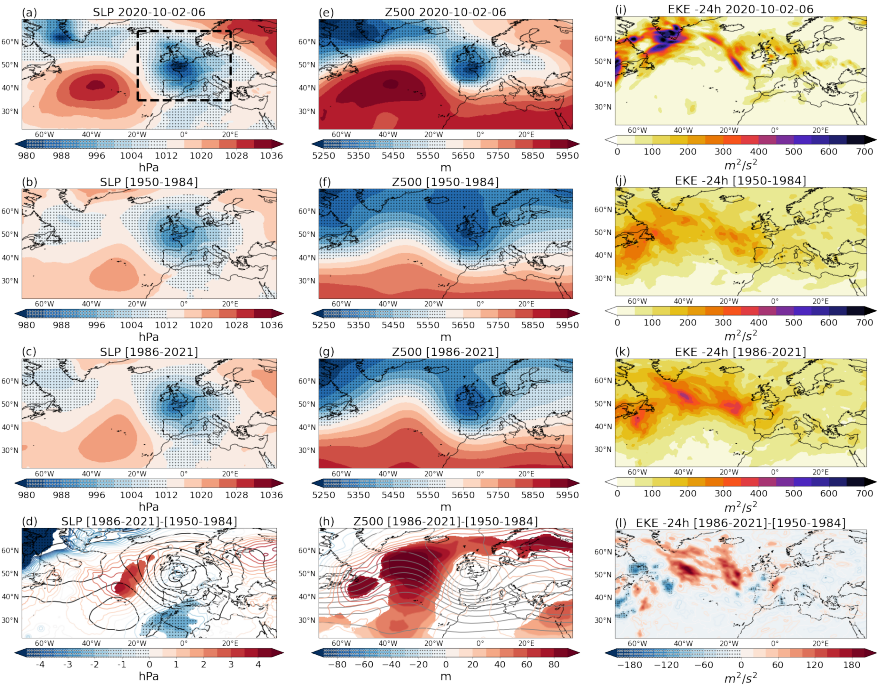

Fig. 2 Mean sea-level pressure (a) and geopotential height at 500hPa (e) at the *lag 0* date of storm Alex and 500 hPa eddy kinetic energy (i) 24 hours prior to the *lag 0*. SLP composites of the 30 analogue storms for the counterfactual (b) and factual (c) periods, and the corresponding Z500 (f,g) and EKE500 (j,k) composites. Factual minus counterfactual differences of SLP (d), Z500 (h) and EKE500 (l). Coloured contours in (d) and (h) show the differences while grey contours show the counterfactual absolute values. Shading in (d, h, l) shows statistically significant differences. In all panels, negative and low values are stippled

in the SLP and Z500 maps (Fig. 2d,h). Figure 2l also shows an increase of the maximum EKE500 over most of the North Atlantic, which implies that storms in the factual period are more energetic in their growth phase than those in the earlier period.

4.2 Cyclone tracking

To better assess changes in storm location, the tracks of the analogue cyclones are shown in Fig. 4. There is a clear latitudinal shift in the backward trajectories, that is, the trajectories of the cyclones up to 48 hours before the *lag 0* dates: in the factual period (solid red), the storms head towards Europe from higher latitudes than those in the counterfactual period (dashed blue). There is no overlap in the confidence intervals, which means that this shift is statistically significant. The forward trajectory response, that is, up to 48 hours after the *lag 0* dates, is less clear, as most storms dissipate not far upstream of the English Channel. The backward trajectory of Alex shows that

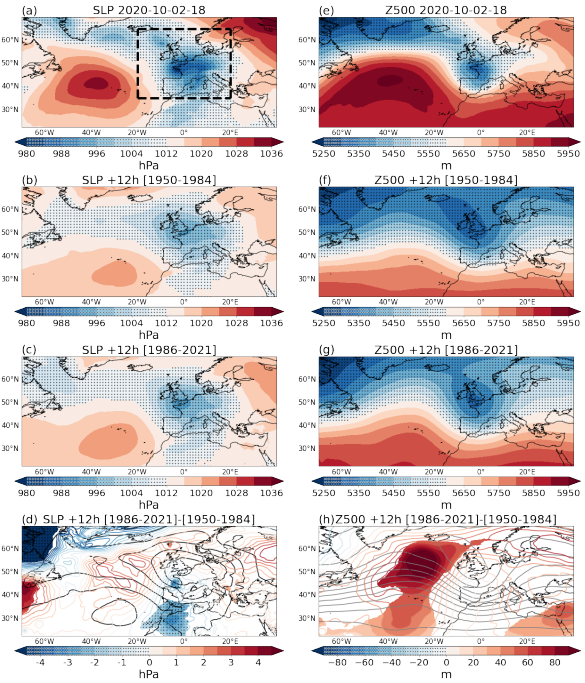

Fig. 3 Same Fig. 2a–h, but at *lag +12* dates.

the cyclone formed and grew at latitudes below 50°N (Fig. 4), indicating a higher resemblance with those in the counterfactual period.

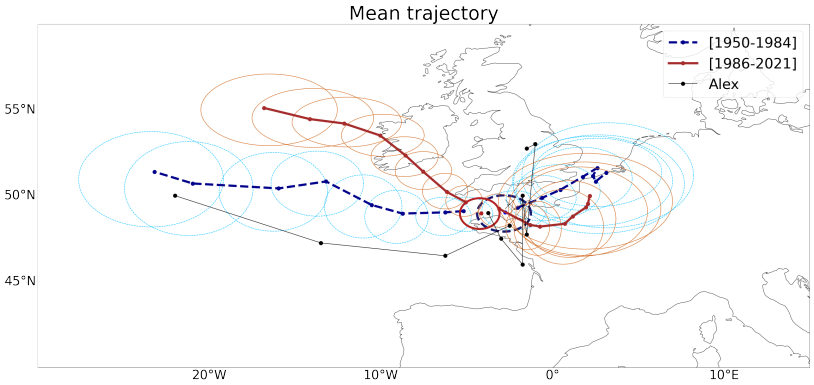

Fig. 4 Alex's track (black line) and average cyclone tracks for the factual (red solid line) and counterfactual (blue dashed line) periods. Dots represent cyclone locations on 6-hourly timesteps. Ellipses show the confidence interval, built using bootstrapping, for each timestep of factual (red thin solid lines) and counterfactual (blue thin dashed lines): the x-axis shows confidence intervals of longitudes and the y-axis of latitudes. Thick ellipses and dots show the confidence intervals and the average cyclone positions for the dates of the analogues, respectively.

A counting of explosive cyclones using the definition of Sanders and Gyakum (1980) has been performed for both periods. In the counterfactual period two analogue cyclones underwent explosive cyclogenesis, from 11/03/1976 at 6 AM to 12/03/1976 at 6 PM and from 03/10/1984 at 12 AM to 04/10/1984 at 12 PM. The latter corresponds to storm Hortense, which mainly affected Southwestern France (Météo France, 2019a). In the factual period, apart from Alex itself only one explosive cyclone has been found, from 04/11/2000 at 12 AM to 05/11/2000 at 18 PM. This is cyclone Rebekka, which had its greatest impact in Southern France (Météo France, 2019b). The NDRs of the two explosive cyclones in the counterfactual period (1.51 and 1.50, respectively) are larger than that of the single explosive cyclone in the factual period (1.20). Alex has the largest NDR of our cyclone sample (1.61). The results presented here only include a very small fraction of the North Atlantic cyclones, and the explosive cyclone analogues found take place over a short period of time, between the 1974 and 2000, which is not enough to attribute the decline (from 2 explosive cyclones to 1) to any specific factor. A counting of cyclones that ended in the Mediterranean region has also been done, and we find 3 in the counterfactual world and 5 in the factual. This increase in frequency may be linked to the increase in waviness seen previously, although the results found here are insufficient to draw conclusions on the tendency of the number of Atlantic cyclones reaching the Mediterranean.

4.3 Seasonality of analogues

Figure 5a,b shows that in the counterfactual period Alex-like storms were more common in spring while in factual conditions they occur chiefly in autumn. The number of analogues in winter and summer remains unchanged over the two periods.

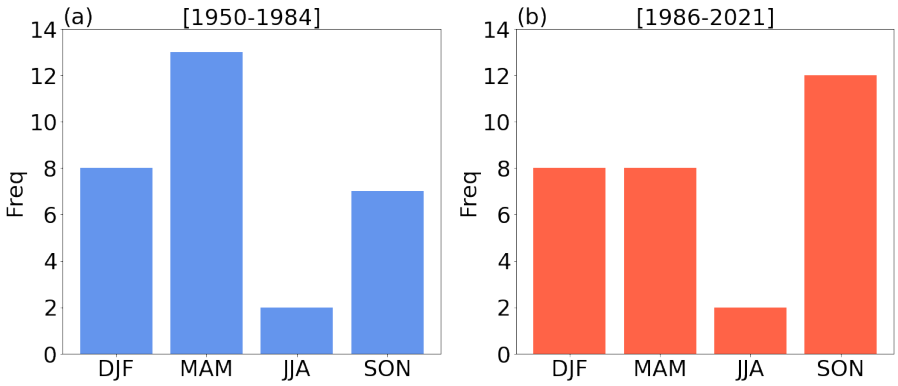

Fig. 5 Frequency of analogues per season, namely winter (DJF), spring (MAM), summer (JJA) and autumn (SON), for the counterfactual (a) and factual (b) periods.

The dynamical changes observed in figure 2d,h,l and 4, i.e., a wavier pressure pattern, a strengthening of the eddy activity, and a poleward shift of the backward trajectories, may be linked to either a direct or an indirect climate change signal. In the former, climate change would act to shift poleward and strengthen Alex's analogues directly. In the latter, climate change leads to a seasonal shift in the occurrence of analogue storms, and the observed changes correspond to the changes in the mean behavior of the cyclones according to the season of most frequent occurrence. The two effects are not exclusive, and changes may reflect a combination of direct and indirect signals. To help evaluate these two hypotheses, we search for 30 analogue storms in autumn (September-October-November) and 30 in spring (March-April-May) for each period and repeat the analysis of Sect. 4.1 and 4.2. Z500 field shows a wavier pattern, that is, a northward extension of the high pressure systems, in the factual period during autumn (Fig. B6), while in spring the pattern is less clear (Fig. B7). SLP maps show a deepening of the cyclone over France in autumn, and again a less clear pattern in spring. Hence, we attribute the wavier pattern and the increase in cyclone depth to: (i) a seasonal shift of the analogues from spring to autumn; and (ii) changes in autumn pressure patterns, when Alex occurred. This response could be then a combination of: (i) an indirect and (ii) a direct climate change signal, even though the proportion of (i) and (ii) is difficult to quantify. The mean tracking shows a clear poleward shift of backward and forward trajectories in spring, while in autumn the shift is weaker (Fig. B8).

4.4 Quality of Analogues

Figure 6a,b shows that composite SLP anomalies over the North Atlantic are smaller in the factual than in the counterfactual period. Figure 6c shows the distributions of the analogues quality. The set of factual cyclones provides better analogues than the cyclones from the counterfactual period. We also compute pressure anomalies and analogues quality for spring and autumn analogues separately (Fig. B9 and B10, respectively). Spring anomalies are larger over the North Atlantic compared to autumn ones in both periods. In the counterfactual period, analogues quality is better in spring than in autumn, which highlights the similarity of Alex with spring storms. In other words, Alex is more similar to analogue cyclones in spring in the counterfactual period, while the North Atlantic atmospheric circulation pattern associated with Alex is closer to that of the autumn analogues, consistent with the pressure field seasonality (Alex occurred in October). However, the quality of autumn analogues improves significantly in the factual world, while in spring there is almost no difference between the counterfactual and factual periods. We thus conclude that Alex was a "black swan" in autumn in the counterfactual period, and rather reflected the characteristics of spring cyclones. However, in the factual period the number of autumn analogues is rising (Fig. 5) and the quality is improving.

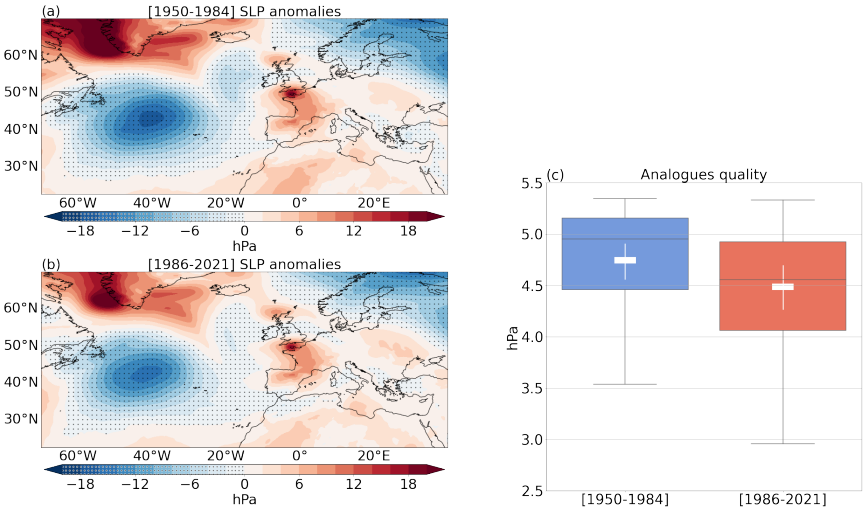

Fig. 6 Sea-level pressure anomalies of counterfactual (a) and factual (b) periods, and boxplots of analogues quality (c). The white horizontal lines show the means of each distribution and the white vertical lines the corresponding confidence intervals.

4.5 Impacts

In this section, we evaluate three surface fields to detect differences between factual and counterfactual impacts: PR, T2M and WG.

Alex generated heavy precipitation in southern and eastern France and northern Italy (Fig. 7a). The analogues averages (Fig. 7b,c) also show a significant amount of precipitation over this region in both periods, although much lower than storm Alex. There is also much weaker precipitation in southern England, central France and Northern Spain compared to Alex. This may be ascribed to a combination of weaker analogue cyclones and some variability in their position that leads to aliasing in the composite. Figure 7d shows a significant increase in precipitation between the counterfactual and factual analogues of more than 12 mm in 24 hours windward of the Alps, a region that suffered catastrophic consequences from Alex.

The increase in rainfall, probably linked to the Stau effect, is accompanied by a rise in 2m air temperature (Fig. 7h) leeward of the Alps, linked to the Foehn effect. In addition, there is a significant increase in temperature by more than 1.5 K over the eastern Mediterranean, the northeastern Atlantic Ocean, and the Baltic Sea. This increase can be due to a direct climate change signal, or it can reflect a shift in the seasonality of the analogues. To better assess these changes, we repeated the analysis on the deseasonalized T2M field (Fig. B11). We did not find significant changes between the counterfactual and factual periods, meaning that the T2M signal over the Alps and sea regions is mainly due to a shift in seasonality.

Figure 7l shows an increase of the 10m maximum wind gust in the Alps, Liguria and Provence of up to 5 m/s. Increasing accumulated precipitation

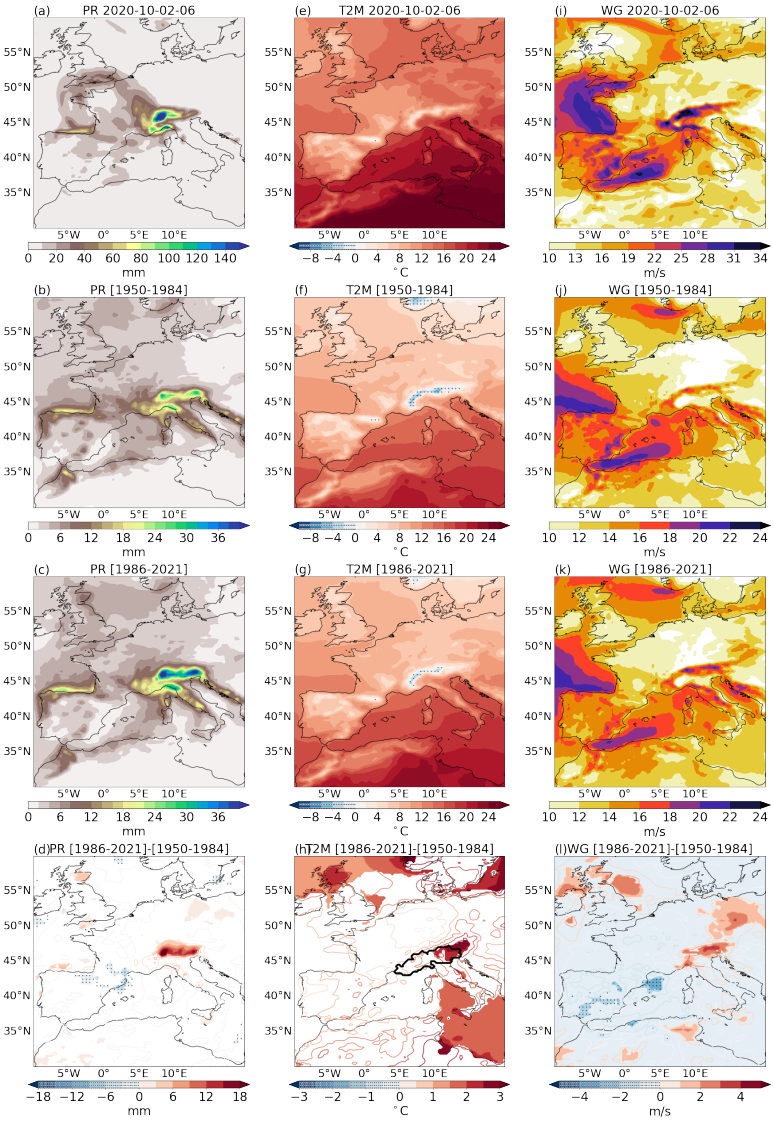

Fig. 7 24-hour accumulated precipitation for Alex (PR, a), counterfactual analogues (b), factual analogues (c), and difference between the two periods (d). Daily average of 6-hourly 2-meter air temperature for Alex (T2M, e), counterfactual analogues (f), factual analogues (g), and difference between the two periods (h). Maximum 10m wind gust within 24 hours for Alex (WG,i), counterfactual analogues (j), factual analogues (k), and difference between the two periods (l). Note that color bars in (a),(i) and (b,c),(j,k) are different. The thick black contour in (h) shows the spatial mask applied in the analysis of Fig. 8 and covers the *target region* formed by: Provence-Alpes-Côte d'Azur, Liguria, Piemonte, Lombardia, Valle d'Aoste, Provincia Autonoma di Bolzano, Veneto, Provincia Autonoma di Trento and Friuli-Venezia Giulia.

and maximum wind gust imply that factual cyclones are a greater hazard. 24-hour mean 10m meridional wind (Fig. B12) shows positive anomalies over the Ligurian Sea and the Gulf of Venice, which enhances the advection of warm, humid air from the Mediterranean to Northern Italy and Southeastern France (Fig. B12h). This increase in meridional wind, related to an increase in the meridional SLP gradient, can also yield the increase in precipitation seen previously (Fig. 7d, h).

To further quantify the observed increase in precipitation and temperature in northern Italy and southern France, we first apply a spatial mask (Fig. 7h) to limit the analysis to the regions of highest impacts for Alex and greater differences between the counterfactual and factual analogues. This delimited region is referred to as *target region* in the remaining text. For Alex's *lag 0* time step, we compute the 99th quantile of PR, T2M and WG over the *target region*. We then compute the (spatial) average values above this quantile in the *target region*. This procedure is also applied to the analogues. We term the (spatial) averages maximum precipitation (PRmax), maximum temperature (T2Mmax) and maximum wind gust (WGmax). Hence, we can determine the different probability distributions of PRmax, T2Mmax and WGmax, linked to an Alex-like storm, in the two periods (counterfactual and factual; Fig. 8). We find that PRmax during Alex is much higher than the rest of the analogues, reaching almost 250 mm. The means of PRmax for the analogues are around 50 mm in the counterfactual period and 80 mm in the factual period. In addition, in the factual period the 75% quantile of the boxplot exceeds 100 mm of rain, while it barely reaches 60 mm in the counterfactual. Hence, in the factual period there is an increase in maximum rainfall. T2Mmax during Alex is higher than that of most of its analogues. There is also a shift of the T2Mmax distribution towards higher maximum temperatures in factual conditions by about 2°C. WGmax during Alex is higher than that of the analogues in factual world but comparable with the counterfactual maximum. WGmax mean and median values increase from counterfactual to factual periods by about 2 m/s. PRmax distribution differences between the two periods are statistically significant, while the T2Mmax and WGmax differences are not. We repeated the analysis of Fig. 8 but for the full domain to find the analogues (dashed-line box in Fig. 1), and applying a land-sea mask for the wind gusts. We have found qualitatively different results for the wind gusts but similar for precipitation (not shown). In the case of wind gusts, the differences in the probability distributions are likely due to features of the synoptic circulation away from the *target region*. We found that 8 analogues in the counterfactual period and 12 in the factual have their highest wind gusts over the *target region*. Regarding the precipitation, the region of maximum precipitation of most of the analogues, that is, 22 in the counterfactual period and 25 in the factual, corresponds to the region of highest precipitation of Alex.

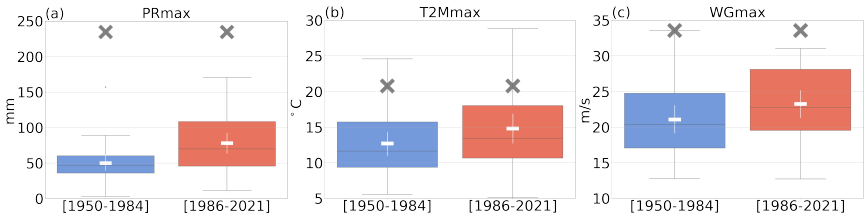

Fig. 8 Boxplot of the area-averaged values above the 99% quantile over the *target region* for PR (a), T2M (b) and WG (c). The white horizontal lines show the means of each distribution and the white vertical lines the corresponding confidence intervals. Grey crosses show the values of Alex.

4.6 Dynamical system metrics

Table 1 shows a decrease in d in the factual world with respect to the counterfactual, which means that the most recent climate has fewer possible evolutions than the counterfactual one. In addition, θ^{-1} shows that factual period storms are ∼4 hours more persistent than the counterfactual period ones (Table 1). Hence, the sea-level pressure pattern is more persistent in the factual period, increasing the stationarity of the cyclonic systems. The differences in d and θ^{-1} are both statistically significant. The decrease in d and the increase in θ^{-1} point to an increase in the intrinsic predictability, as low values of d and high of θ^{-1} are associated with high-predictability configurations (Messori et al, 2017; Faranda et al, 2017; Hochman et al, 2019). While this result is obtained specifically for severe cyclones, it is in line with the results found in Faranda et al (2019) and Scher and Messori (2019) who, using two independent approaches, argued for an increasing predictability of the midlatitude atmosphere.

	[1950-1984]	**[1986-2021]**	**Change %**
d	7.5 [6.6 8.3]	6.8 [6.1 7.6]	-8.5
θ^{-1}	20.8 [18.9 22.7]	24.1 [21.4 26.8]	15.7

Table 1 Local dimension d (unitless) and persistence θ^{-1} (hours) in the counterfactual (first column) and factual (second column) periods, and the relative changes in the factual with respect to the counterfactual period (third column). Values in brackets show confidence intervals.

5 Discussion and Conclusion

We have presented a methodology for the attribution of severe extratropical cyclones and their impacts to ongoing climate change. We specifically applied this to storm Alex, which struck southern and western Europe in October 2020. We based our analysis on 30 analogue storms (Yiou, 2014) for Alex in factual (with strong climate change) and counterfactual (with limited climate change) periods from ERA5, and their dynamical properties.

A comparison of the two sets of analogues evidences that the factual storms typically occur on the background of a wavier atmospheric pattern than the counterfactual storms. This stronger meridional component of the flow is likely linked to a slower-moving wave pattern (Screen and Simmonds, 2014), as also highlighted by a persistence index we computed using dynamical system theory. This shows an average 4h increase in the persistence of atmospheric patterns in the factual world. Previous studies also found an increase in persistent circulation regimes in recent years (Alvarez-Castro et al, 2018; Hoffmann, 2018), and some suggest a possible link with Arctic Amplification (Cohen et al, 2018; Yao et al, 2017; Kornhuber and Tamarin-Brodsky, 2021). The observed amplified low-level warming at high latitudes in the NH (Serreze et al, 2009) would act to weaken the zonal wind via the thermal wind relationship, resulting in an increase in amplitude of the polar jet meandering and slower wave propagation, and favouring the longer persistence of weather patterns that lead to extreme events. However, due to the complexity of the eddy-mean flow feedbacks, the underlying dynamics are not entirely clear (Hoskins and Woollings, 2015). In addition, a challenge arises in distinguishing the forced signal from the internal variability (Mann et al, 2017; Barnes and Screen, 2015), partly due to an incomplete knowledge of the influence of high-latitudes on mid-latitude weather as well as a lack of data (Cohen et al, 2014). Hence, according to the last IPCC report, "there is low to medium confidence in the exact role and quantitative effect of historical Arctic warming and sea-ice loss on mid-latitude atmospheric variability" (Doblas-Reyes et al, 2021). Further analysis linking sea-ice loss with the present work's findings could be performed, although the lack of reliable sea ice data before 1978 complicates the study.

We further find that, in the factual period, cyclones like Alex are more energetic in their growth phase, as seen by an increase in the eddy kinetic energy at *lag -24* hours. They also display lower pressures at *lag +12* hours during the decay phase of the storms. This interpretation assumes that *lag 0* corresponds also to the mature stage for the analogues of Alex. The analogues also tend to occur more frequently in autumn and less frequently in spring. However, this does not imply an a priori influence on storm intensity, as the two seasons are comparable in this respect (Hoskins and Hodges, 2019). When separating analogues according to season, autumn analogues have been found to undergo a large increase in cyclone intensity, which may be related to an increase in humidity leading to an increase in moist baroclinic instability and maximum EKE500 of baroclinic eddies (Gutowski Jr et al, 1992). Sinclair and Watterson (1999) also suggests that an enhancement in water vapor content and a localized increase in baroclinicity could increase regional storm activity. In addition, an increase of the land-sea contrast due to a faster warming over land than over the ocean (Jia et al, 2019) could enhance baroclinicity in summer and early autumn, yielding to an increase of the cyclones intensity. Further investigation using ad hoc numerical model simulations would be required to analyse this and discern the main sources of increased baroclinicity.

A poleward shift in the factual period of the eddy activity prior to the storms and of the backward trajectories has been found. According to Hoskins and Hodges (2019), in autumn the main North Atlantic storm track is located farther poleward than in spring. Hence, the poleward shift of the trajectories could be explained by a higher frequency of storms in autumn, as an indirect climate change signal. There is also a weak poleward shift of the backward trajectories in autumn, which acts as a direct climate change signal. However, we have also found that it is in spring when this poleward shift is greatest. In addition, the wavier pressure field configuration may act to deflect cyclones poleward over the North Atlantic. We thus deduce that the poleward shift is due to a combination of: (i) a direct climate change that shifts poleward the storms, especially in spring, probably due to a poleward shift of the region of maximum baroclinicity; (ii) an indirect signal, whereby analogues become more common in autumn when the cyclones are located further poleward; and (iii) wavier pressure patterns that deflect cyclones. Further analysis must be performed to evaluate each components' contribution to the observed poleward shift of the cyclones. A future pathway could be to create analogues based on the cyclone tracks.

Finally, an increase in precipitation in Northern Italy has been detected in the factual period, along with an increase in low-level temperature in the same region and wind gust over the Alps, Liguria and Provence. This result is in agreement with Reale et al (2022) and Zappa et al (2015), who, using climate models, found that the cyclone-related precipitation rate and wind speed will increase in the central Mediterranean region in a warmer climate. The increase in precipitation in Northern Italy could have a thermodynamic origin, linked to temperature by the Clausius Clapeyron relation, and a dynamic origin, related to the meridional wind and the orographically induced Stau effect. Deseasonalized temperature differences show that the temperature signal corresponds mainly to a seasonal shift of the analogues, which suggests that the increase in precipitation could be related to the shift from spring to autumn cyclones. Hence, in a warmer climate, hazardous Alex-like storms may become more likely, as they occur more frequently in the fall when the Mediterranean is warmer and the air is moister than in spring. The increase in southerly advection by 10m meridional wind has a dynamic origin, as storms have lower core pressures at *lag +12* dates in the factual climate. Southerly winds advect humid air from the Mediterranean, and together with the orographic forcing by the Alps, can increase precipitation. Hence, given the differences observed in the surface fields, more flooding could be triggered at the base of the Alps, the region that suffered the largest impacts during the Alex.

To summarize, our results show a more persistent atmospheric pattern for Alex-like cyclones in a warmer climate. Both signals indicate that the cyclones remain over the same region for longer, favouring extreme events that result from prolonged weather conditions. There is also an increase in the maximum eddy kinetic energy during their development and the cyclones display lower pressures during their decay phase. In addition, in the factual period,

Alex's analogues produce more precipitation in Northern Italy, and specifically along the southward flank of the Alps, which could trigger more severe flooding events. We emphasize that our findings do not explicitly demonstrate that the observed changes are entirely anthropogenically-driven, and they may also be influenced by the internal variability of the climate system. A large sample of model data would be required to adequately isolate the impact of anthropogenic radiative forcing.

The approach used in this work to attribute storm Alex and its impacts to climate change combines several techniques, including the analogues method (Yiou, 2014), dynamical systems theory (Faranda et al, 2017), and extreme event attribution (Stott et al, 2016), to provide a novel, complete toolkit for attribution studies. This toolkit may be applied with profit to other severe extra-tropical and tropical cyclones, and provide new insights on the influence of climate change on extreme weather phenomena.

Statements and declarations

- Funding: This project has received funding from the European Union's Horizon 2020 research and innovation programme under the Marie Sklodowska-Curie grant agreement N° 956396 (EDIPI project).
- Conflict of interest: The authors declare no conflict of interest.
- Ethics approval: Not applicable.
- Consent to participate: Not applicable.
- Consent for publication: Not applicable.
- Availability of data and materials: ERA5 data are available on the C3S Climate Data Store at https://cds.climate.copernicus.eu/#!/home.
- Code availability: The main results of this work were obtained using Python. The scripts are available upon request.
- Authors' contributions: MG performed the analysis. MG and DF co-designed the analyses. All authors participated to drafting and reviewing the manuscript.

References

Allan RP, Hawkins E, Bellouin N, et al (2021) IPCC, 2021: Summary for Policymakers. In Climate Change 2021: The physical science basis. Contribution of Working Group I to the Sixth Assessment Report of the Intergovernmental Panel on Climate Change [Masson-Delmotte, V., P. Zhai, A. Pirani, S.L. Connors, C. Péan, S. Berger, N. Caud, Y. Chen, L. Goldfarb, M.I. Gomis, M. Huang, K. Leitzell, E. Lonnoy, J.B.R. Matthews, T.K. Maycock, T. Waterfield, O. Yelekçi, R. Yu, and B. Zhou (eds.)]. Cambridge University Press. In Press.

Alvarez-Castro MC, Faranda D, Yiou P (2018) Atmospheric dynamics leading to West European summer hot temperatures since 1851. Complexity 2018:2494,509. https://doi.org/10.1155/2018/2494509

Aon (2020) Global Catastrophe Recap: October 2020. Available at: http://thoughtleadership.aon.com/documents/20201111_analytics-if-october-global-recap.pdf Accessed: October 202O

Barnes EA, Screen JA (2015) The impact of arctic warming onthe midlatitude jet-stream: Can it? has it? will it? WIREs Clim Change 6:277–286. https://doi.org/https://doi.org/10.1002/wcc.337

Cattiaux J, R. Vautard CC, Yiou P, et al (2010) Winter 2010 in europe: A cold extreme in a warming climate. Geophysical Research Letters 37. https://doi.org/https://doi.org/10.1029/2010GL044613

Chang E, Yau A (2016) Northern hemisphere winter storm track trends since 1959 derived from multiple reanalysis datasets. Climate Dynamics 47:1435–1454. https://doi.org/https://doi.org/10.1007/s00382-015-2911-8

Chang EKM, Ma CG, Zheng C, et al (2016) Observed and projected decrease in northern hemisphere extratropical cyclone activity in summer and its impacts on maximum temperature. Geophysical Research Letters 43:2200–2208

Cohen J, Screen JA, Furtado JC, et al (2014) Recent arctic amplification and extreme mid-latitude weather. Nature Geoscience 7:627–637. https://doi.org/https://doi.org/10.1038/ngeo2234

Cohen J, Zhang X, Francis J, et al (2018) Arctic change and possible influence on mid-latitude climate and weather: a us clivar white paper. US CLIVAR reports

Doblas-Reyes F, Sörensson A, Almazroui M, et al (2021) Linking global to regional climate change. In Climate Change 2021: The physical science basis. Contribution of Working Group I to the Sixth Assessment Report of the Intergovernmental Panel on Climate Change [Masson-Delmotte, V., P. Zhai, A. Pirani, S.L. Connors, C. Péan, S. Berger, N. Caud, Y. Chen, L. Goldfarb, M.I. Gomis, M. Huang, K. Leitzell, E. Lonnoy, J.B.R. Matthews, T.K. Maycock, T. Waterfield, O. Yelekçi, R. Yu, and B. Zhou (eds.)]. Cambridge University Press. In Press.

European State of the Climate (2020) Storm Alex. Available at https://climate.copernicus.eu/esotc/2020/storm-alex

Eurostat (2021) NUTS - Nomenclature of territorial units for statistics. https://ec.europa.eu/eurostat/web/nuts/background

Faranda D, Messori G, Yiou P (2017) Dynamical proxies of North Atlantic predictability and extremes. Scientific Reports https://doi.org/10.1038/srep41278, URL https://hal.archives-ouvertes.fr/hal-01340301

Faranda D, Alvarez-Castro M, Messori G, et al (2019) The hammam effect or how a warm ocean enhances large scale atmospheric predictability. Nat Commun 10:1316. https://doi.org/https://doi.org/10.1038/s41467-019-09305-8

Feser F, Barcikowska M, Krueger O, et al (2015) Storminess over the north atlantic and northwestern europe—a review. Quarterly Journal of the Royal Meteorological Society 141(687):350–382. https://doi.org/https://doi.org/10.1002/qj.2364, URL https://rmets.onlinelibrary.wiley.com/doi/abs/10.1002/qj.2364, https://arxiv.org/abs/https://rmets.onlinelibrary.wiley.com/doi/pdf/10.1002/qj.2364

Freitas ACM, Freitas JM, Todd M (2008) Hitting time statistics and extreme value theory. https://doi.org/10.48550/ARXIV.0804.2887

Gulev S, Thorne P, Ahn J, et al (2021) Changing state of the climate system. In Climate Change 2021: The physical science basis. Contribution of Working Group I to the Sixth Assessment Report of the Intergovernmental Panel on Climate Change [Masson-Delmotte, V., P. Zhai, A. Pirani, S.L. Connors, C. Péan, S. Berger, N. Caud, Y. Chen, L. Goldfarb, M.I. Gomis, M. Huang, K. Leitzell, E. Lonnoy, J.B.R. Matthews, T.K. Maycock, T. Waterfield, O. Yelekçi, R. Yu, and B. Zhou (eds.)]. Cambridge University Press. In Press.

Gutowski Jr WJ, Branscome LE, Stewart DA (1992) Life cycles of moist baroclinic eddies. Journal of Atmospheric Sciences 49:306–319

Harvey BJ, Cook P, Shaffrey L, et al (2020) The response of the Northern Hemisphere storm tracks and jet streams to climate change in the CMIP3, CMIP5, and CMIP6 climate models. Journal of Geophysical Research: Atmospheres 125. https://doi.org/https://doi.org/10.1029/2020JD032701

Hersbach H, Bell B, Berrisford P, et al (2020) The ERA5 global reanalysis. Quat J Roy Met Soc 146(730):1999–2049. https://doi.org/https://doi.org/10.1002/qj.3803, iSBN: 0035-9009 Publisher: Wiley Online Library

Hochman A, Alpert P, Harpaz T, et al (2019) A new dynamical systems perspective on atmospheric predictability: Eastern mediterranean weather regimes as a case study. Science advances 5(6):eaau0936

Hoffmann P (2018) Enhanced seasonal predictability of the summer mean temperature in central europe favored by new dominant weather patterns. Climate dynamics 50(7):2799–2812

Hoskins B, Woollings T (2015) Persistent extratropical regimes and climate extremes. Curr Clim Change Rep 1:115–124. https://doi.org/10.1007/s40641-015-0020-8

Hoskins BJ, Hodges KI (2019) The annual cycle of Northern Hemisphere storm tracks. Part II: Regional detail. Journal of Climate 32:1761–1775. https://doi.org/http://dx.doi.org/10.1175/jcli-d-17-0871.1

Jézéquel A, Yiou P, Radanovics S (2018) Role of circulation in european heatwaves using flow analogues. Climate dynamics 50(3):1145–1159

Jia G, Shevliakova E, Artaxo P, et al (2019) Land–climate interactions. In: Climate Change and Land: an IPCC special report on climate change, desertification, land degradation, sustainable land management, food security, and greenhouse gas fluxes in terrestrial ecosystems [P.R. Shukla, J. Skea, E. Calvo Buendia, V. Masson-Delmotte, H.-O. Pörtner, D.C. Roberts, P. Zhai, R. Slade, S. Connors, R. van Diemen, M. Ferrat, E. Haughey, S. Luz, S. Neogi, M. Pathak, J. Petzold, j. portugal pereira, P. Vyas, E. Huntley, K. Kissick, M. Belkacemi, J. Malley, (eds.)]. In press.

Kornhuber K, Tamarin-Brodsky T (2021) Future Changes in Northern Hemisphere Summer Weather Persistence Linked to Projected Arctic Warming. Geophysical Research Letters 48. https://doi.org/https://doi.org/10.1029/2020GL091603

Lee JY, Marotzke J, Bala G, et al (2021) Future global climate: Scenario-based projections and near-term information. In Climate Change 2021: The physical science basis. Contribution of Working Group I to the Sixth Assessment Report of the Intergovernmental Panel on Climate Change [Masson-Delmotte, V., P. Zhai, A. Pirani, S.L. Connors, C. Péan, S. Berger, N. Caud, Y. Chen, L. Goldfarb, M.I. Gomis, M. Huang, K. Leitzell, E. Lonnoy, J.B.R. Matthews, T.K. Maycock, T. Waterfield, O. Yelekçi, R. Yu, and B. Zhou (eds.)]. Cambridge University Press. In Press

Lucarini V, Faranda D, Wouters J (2012) Universal Behaviour of Extreme Value Statistics for Selected Observables of Dynamical Systems. https://doi.org/10.1007/s10955-012-0468-z

Lucarini V, Faranda D, Freitas ACM, et al (2016) Extremes and recurrence in dynamical systems. https://doi.org/https://doi.org/10.48550/arXiv.1605.07006, 1605.07006

Luu LN, Vautard R, Yiou P, et al (2018) Attribution of extreme rainfallevents in the South of France using EURO-CORDEX simulations. Geophysical Research Letters 45:6242–6250. https://doi.org/https://doi.org/10.1029/2018GL077807

Mann ME, Rahmstorf S, Kornhuber K, et al (2017) Influence of anthropogenic climate change on planetary wave resonance and extreme weather events. Scientific Reports 7. https://doi.org/10.1038/srep45242

Messori G, Caballero R, Faranda D (2017) A dynamical systems approach to studying midlatitude weather extremes. Geophysical Research Letters 44(7):3346–3354. https://doi.org/https://doi.org/10.1002/2017GL072879, URL https://agupubs.onlinelibrary.wiley.com/doi/abs/10.1002/2017GL072879, https://arxiv.org/abs/https://agupubs.onlinelibrary.wiley.com/doi/pdf/10.1002/2017GL072879

Messori G, Harnik N, Madonna E, et al (2021) A dynamical systems characterization of atmospheric jet regimes. Earth System Dynamics 12(1):233–251

Moon W, Manucharyan GE, Dijkstra HA (2021) Baroclinic instability and large-scale wave propagation in a planetary-scale atmosphere. https://doi.org/https://doi.org/10.1002/qj.4232

Météo France (2019a) Tempête Hortense du 4 octobre 1984. Available at http://tempetes.meteofrance.fr/IMG/anthemis_pdf/19841004.pdf

Météo France (2019b) Tempête Rebekka du 6 novembre 2000. Available at http://tempetes.meteo.fr/IMG/anthemis_pdf/20001106.pdf

Météo France (2020a) Bulletin climatique octobre 2020. Available at https://donneespubliques.meteofrance.fr/donnees_libres/bulletins/BCM/202010.pdf

Météo France (2020b) Tempête Alex: des intempéries exceptionnelles. Available at https://meteofrance.com/actualites-et-dossiers/climat/tempete-alex-des-intemperies-exceptionnelles

Météo France (2021) Tempête Alex du 2 octobre 2020. Available at http://tempetes.meteo.fr/IMG/anthemis_pdf/20201002.pdf

National Academies of Sciences, Engineering, and Medicine (2016) Attribution of Extreme Weather Events in the Context of Climate Change. The National Academies Press, Washington, DC, https://doi.org/10.17226/21852, URL https://www.nap.edu/catalog/21852/attribution-of-extreme-weather-events-in-the-context-of-climate-change

Neu U, Akperov MG, Bellenbaum N, et al (2013) IMILAST: A community effort to intercompare extratropical cyclone detection and tracking algorithms. Bulletin of the American Meteorological Society Bulletin of the American Meteorological Society 94:529–547. https://doi.org/https://doi.org/10.1175/BAMS-D-11-00154.1

Pall P, Aina T, Stone DA, et al (2011) Anthropogenic greenhouse gas contribution to flood risk in england and wales in autumn 2000. Nature 470:382–385. https://doi.org/10.1038/nature09762

Parker DJ (1998) Secondary frontal waves in the north atlantic region: A dynamical perspective of current ideas. Quarterly Journal of the Royal Meteorological Society 124(547):829–856. https://doi.org/https://doi.org/10.1002/qj.49712454709, URL https://rmets.onlinelibrary.wiley.com/doi/abs/10.1002/qj.49712454709, https://arxiv.org/abs/https://rmets.onlinelibrary.wiley.com/doi/pdf/10.1002/qj.49712454709

Philip S, Kew SF, van Oldenborgh GJ, et al (2018) Attribution analysis of the Ethiopian drought of 2015 p 2465–2486. https://doi.org/https://doi.org/10.1175/JCLI-D-17-0274.1

Pinto JG, Spangehl T, Ulbrich U, et al (2005) Sensitivities of a cyclone detection and tracking algorithm: individual tracks and climatology. Meteorologische Zeitschrift 14(6):823–838. https://doi.org/10.1127/0941-2948/2005/0068

Priestley MDK, Catto JL (2022) Future changes in the extratropical storm tracks and cyclone intensity, wind speed, and structure. Weather and Climate Dynamics 3(1):337–360. https://doi.org/10.5194/wcd-3-337-2022

Priestley MDK, Dacre HF, Shaffrey LC, et al (2020) The role of secondary cyclones and cyclone families for the north atlantic storm track and clustering over western europe. Quarterly Journal of the Royal Meteorological Society 146(728):1184–1205. https://doi.org/https://doi.org/10.1002/qj.3733, URL https://rmets.onlinelibrary.wiley.com/doi/abs/10.1002/qj.3733, https://arxiv.org/abs/https://rmets.onlinelibrary.wiley.com/doi/pdf/10.1002/qj.3733

Pörtner HO, Roberts D, Poloczanska E, et al (2022) IPCC, 2022: Summary for policymakers. In: Climate Change 2022: Impacts, Adaptation, and Vulnerability. Contribution of Working Group II to the Sixth Assessment Report of the Intergovernmental Panel on Climate Change

Reale M, Liberato ML, Lionello P, et al (2019) A global climatology of explosive cyclones using a multi-tracking approach. Tellus A: Dynamic Meteorology and Oceanography 71(1):1611,340. https://doi.org/10.1080/16000870.2019.1611340

Reale M, Narvaez WC, Cavicchia L, et al (2022) Future projections of mediterranean cyclone characteristics using the med-CORDEX ensemble of coupled regional climate system models. Climate dynamics 58:2501–2524. https://doi.org/https://doi.org/10.1007/s00382-021-06018-x

Riviera 24 (2021) A quattro mesi dalla tempesta Alex in Costa Azzurra si cercano ancora i corpi delle vittime. Available at: https://www.riviera24.it/2021/02/a-quattro-mesi-dalla-tempesta-alex-in-costa-azzurra-si-cercano-ancora-i-corpi-delle-vit

Accessed: 07/01/2021

Sanders F, Gyakum JR (1980) Synoptic-dynamic climatology of the "bomb". Monthly Weather Review 108:1589–1606. https://doi.org/https://doi.org/10.1175/1520-0493(1980)108⟨1589:SDCOT⟩2.0.CO;2

Scher S, Messori G (2019) How global warming changes the difficulty of synoptic weather forecasting. Geophysical Research Letters 46(5):2931–2939

Screen J, Simmonds I (2014) Amplified mid-latitude planetary waves favour particular regional weather extremes. Nature Climate Change 4:704–709. https://doi.org/10.1038/nclimate2271

Seneviratne S, Zhang X, Adnan M, et al (2021) Weather and climate extreme events in a changing climate. In Climate Change 2021: The physical science basis. Contribution of Working Group I to the Sixth Assessment Report of the Intergovernmental Panel on Climate Change [Masson-Delmotte, V., P. Zhai, A. Pirani, S.L. Connors, C. Péan, S. Berger, N. Caud, Y. Chen, L. Goldfarb, M.I. Gomis, M. Huang, K. Leitzell, E. Lonnoy, J.B.R. Matthews, T.K. Maycock, T. Waterfield, O. Yelekçi, R. Yu, and B. Zhou (eds.)]. Cambridge University Press. In Press.

Serreze MC, Barrett AP, Stroeve JC, et al (2009) The emergence of surface-based arctic amplification. The Cryosphere 3(1):11–19. https://doi.org/10.5194/tc-3-11-2009

Shapiro M, Wernli H, Bao JW, et al (1999) A Planetary-Scale to Mesoscale Perspective of the Life Cycles of Extratropical Cyclones: The Bridge between Theory and Observations, American Meteorological Society, Boston, MA, pp 139–185. https://doi.org/10.1007/978-1-935704-09-6_14, URL https://doi.org/10.1007/978-1-935704-09-6_14

Shaw TA, Baldwin M, Barnes EA, et al (2016) Storm track processes and the opposing influences of climate change. Nature Geosci 9:656–664. https://doi.org/https://doi.org/10.1038/ngeo2783

Sinclair MR, Watterson IG (1999) Objective assessment of extratropical weather systems in simulated climates. Journal of Climate 12(12):3467–3485. https://doi.org/10.1175/1520-0442(1999)012⟨3467:OAOEWS⟩2.0.CO;2

Stott PA, Stone DA, Allen MR (2004) Human contribution to the European heatwave of 2003. Nature 432(7017):610–614. https://doi.org/10.1038/Nature03089

Stott PA, Christidis N, Otto FEL, et al (2016) Attribution of extreme weather and climate-related events. Wiley Interdisciplinary Reviews: Climate Change 7(1):23–41. https://doi.org/10.1002/wcc.380

Süveges M (2007) Likelihood estimation of the extremal index. Extremes 10(1-2):41–55. https://doi.org/10.1063/1.5079656, iSBN: 1386-1999 Publisher: Springer

The Watchers (2020) Death toll caused by storm Alex rises to 15, 21 still missing in france and Italy. Available at: https://watchers.news/2020/10/07/storm-alex-death-toll-damage-october-2020/ Accessed: 07/02/2020

Tilinina N, Gulev SK, Rudeva I, et al (2013) Comparing cyclone life cycle characteristics and their interannual variability in different reanalyses. Journal of Climate 26:6419–6438

Ullrich PA, Zarzycki CM (2017) Tempestextremes: A framework for scale-insensitive pointwise feature tracking on unstructured grids. Geoscientific Model Development 10(3):1069–1090

Ullrich PA, Zarzycki CM, McClenny EE, et al (2021) Tempestextremes v2.1: a community framework for feature detection, tracking, and analysis in large datasets. Geoscientific Model Development 14(8):5023–5048. https://doi.org/10.5194/gmd-14-5023-2021, URL https://gmd.copernicus.org/articles/14/5023/2021/

Vautard R, van Oldenborgh GJ, Otto FEL, et al (2019) Human influence on european winter wind storms such as those of january 2018. Earth System Dynamics 10(2):271–286. https://doi.org/10.5194/esd-10-271-2019

Wallace J, Lim G, Backmon M (1988) Relationship between cyclone tracks, anticyclone tracks and baroclinic waveguides. Journal of Atmospheric Sciences 45:439–462. https://doi.org/https://doi.org/10.1175/1520-0469(1988)045⟨0439:RBCTAT⟩2.0.CO;2

Wilks D (2005) Chapter 5 – Hypothesis Testing. In: Statistical Methods in the Atmospheric Sciences, 2nd edn.

WMO (1987) The measurement of gustiness at routine wind stations — a review. Available at https://library.wmo.int/doc_num.php?explnum_id=7372

WMO (2020) Mediterranean episode causes "unprecedented" rainfall. Available at https://public.wmo.int/en/media/news/mediterranean-episode-causes-unprecedented-rainfall

Yao Y, Luo D, Dai A, et al (2017) Increased quasi stationarity and persistence of winter ural blocking and eurasian extreme cold events in response to arctic warming. part i: Insights from observational analyses. Journal of Climate 30(10):3549 – 3568. https://doi.org/10.1175/JCLI-D-16-0261.1, URL https://journals.ametsoc.org/view/journals/clim/30/10/jcli-d-16-0261.1.xml

Yiou P (2014) Anawege: a weather generator based on analogues of atmospheric circulation. Geoscientific Model Development 7(2):531–543. https://doi.org/10.5194/gmd-7-531-2014

Zappa G, Shaffrey LC, Hodges KI, et al (2013) A multimodel Assessment of Future Projections of North Atlantic and European Extratropical Cyclones in the CMIP5 Climate Models. Journal of Climate 26:5846–5862. https://doi.org/http://dx.doi.org/10.1175/JCLI-D-12-00573.1

Zappa G, Hawcroft MK, Shaffrey L, et al (2015) Extratropical cyclones and the projected decline of winter mediterranean precipitation in the cmip5 models. Climate Dynamics 45(7):1727–1738

Zarzycki CM, Ullrich PA (2017) Assessing sensitivities in algorithmic detection of tropical cyclones in climate data. Geophysical Research Letters 44(2):1141–1149

Appendix A Local dimension d and persistence θ^{-1}

Local dimension d is computed by applying extreme value statistics to Poincaré recurrences of a state ζ (Lucarini et al, 2016). ζ, here represented by Alex's longitude-latitude sea-level pressure map, is a reference point in an appropriately defined phase space. Here, the trajectories in this phase space are successions of 6-hourly sea-level pressure maps in a similar fashion as described in Faranda et al (2017). We then compute the probability that the trajectory returns close to ζ, namely within a ball of radius ϵ centered on ζ. This probability has been studied first by Freitas et al (2008) and obeys an extreme value distribution. In order to compute this probability, we first calculate the distances between ζ and all other points within our dataset as:

$$g(x(t)) = -log(dist(x(t), \zeta)) \tag{A1}$$

where $dist(x(t), \zeta)$ is the Euclidean distance of SLP maps between each timestep $x(t)$ and ζ. The Freitas-Freitas-Todd theorem (Freitas et al, 2008), modified by (Lucarini et al, 2012), states that the probability of recurrences, namely of $x(t)$ to fall inside a ball of radius ϵ and centered at ζ, converges to a Generalized Pareto Distribution:

$$P(z > s(q)) \simeq exp[-\vartheta(\zeta)\frac{z - \mu(\zeta)}{\sigma(\zeta)}] \tag{A2}$$

where $z = g(x(t))$. The radius ϵ is related to a threshold $s(q)$ of the time series of the distances computed as Eq. (A1) by $\epsilon = e^{-s(q)}$. Due to the application of the -log, the exceedances of the threshold are the points that fall within the radius ϵ from ζ. In this work we take q as the 99th percentile of our distance timeseries, so that 1% of the distances exceed the threshold (Fig. B13). The local dimension d is obtained as: $\sigma = 1/d(\zeta)$.

We fit a Generalized Pareto Distribution to the exceedances using the Maximum Likelihood estimator. We also have tested two other methods, the Method of Moments and L-moments, and we have found similar results, namely that when the differences between d in factual and counterfactual periods are statistically significant for a method, they also are so for the others (Fig. B14).

The extremal index ϑ is an adimensional parameter between 0 and 1. Its inverse can be interpreted as the mean residence time of phase-space trajectories within a radius ϵ around ζ in units of the timestep of the data being used, namely a measure of persistence θ. We compute ϑ using the Süveges (2007) estimator.

Appendix B Additional figures

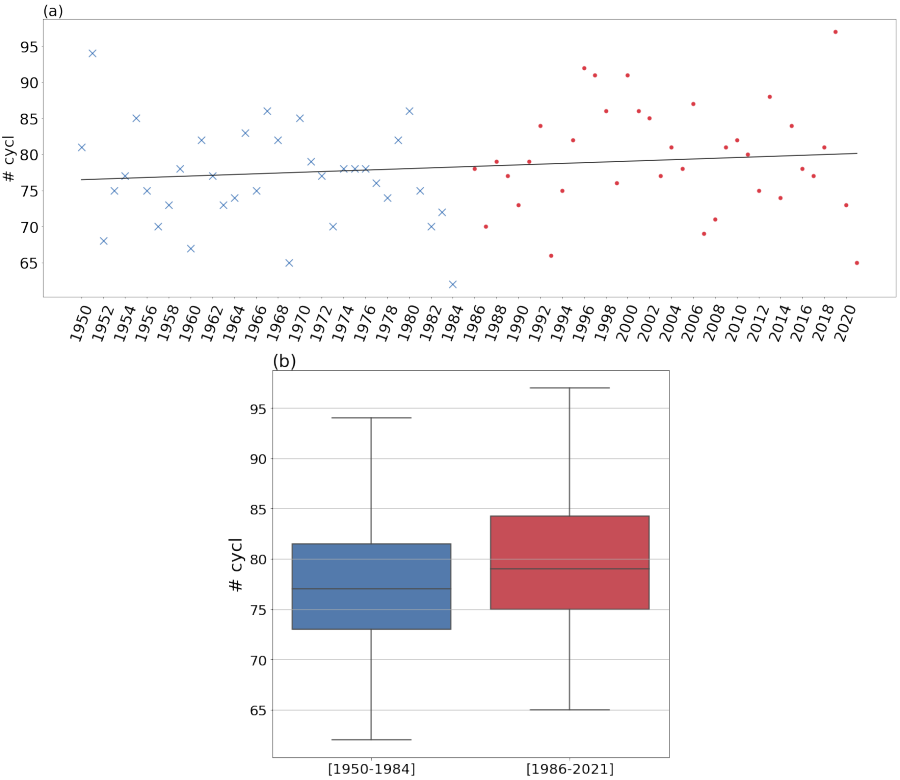

Fig. B1 (a) Number of cyclones over the North Atlantic and western Europe (60W–20E, 30–65N) per year for counterfactual (blue crosses) and factual (brown dots) periods and trend considering the whole period (black line). Cyclones are tracked using the *TempestExtremes* software by Ullrich et al (2021); Ullrich and Zarzycki (2017) using ERA5 data. The customized algorithms in *DetectNodes* and *StitchNodes* codes are almost the same as in Ullrich et al (2021). Cyclones are required to have a closed contour of 2hPa within 6° of the cyclone center, and those with their centers within 6° of one another are merged (*DetectNodes*). Cyclones must persist for at least 60 hours, with a maximum gap of detection of 18 hours, and they must move 12° great-circle distance from the start to the end of the trajectory (*StitchNodes*). (b) Probability distributions of the number of cyclones. The difference in the probability distributions has been tested using the Wilcoxon Rank-Sum test, where the null hypothesis is that the two distributions have equal medians at the 5% significance level, and the alternative hypothesis is that the distribution underlying the factual period is greater than the distribution underlying the counterfactual period. The *p-value* is 0.039, indicating that the median of the factual period is significantly greater than that of the counterfactual period.

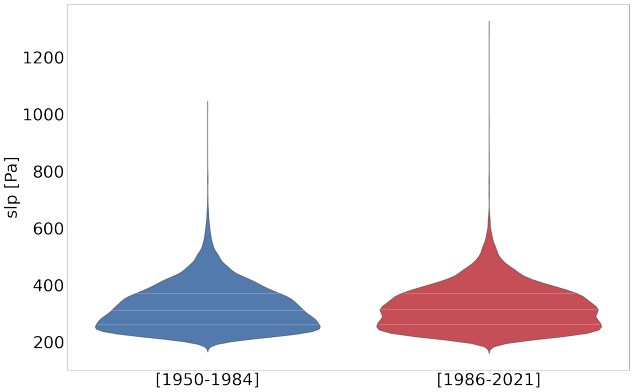

Fig. B2 Probability distribution of the average Euclidean distance between the sea level pressure map of every time step and its 30 closest analogues. The statistical significance of the difference between the distributions is assessed using a two-sample Kolmogorov-Smirnov test with a 5% significance level. No significant differences between the two periods are found.

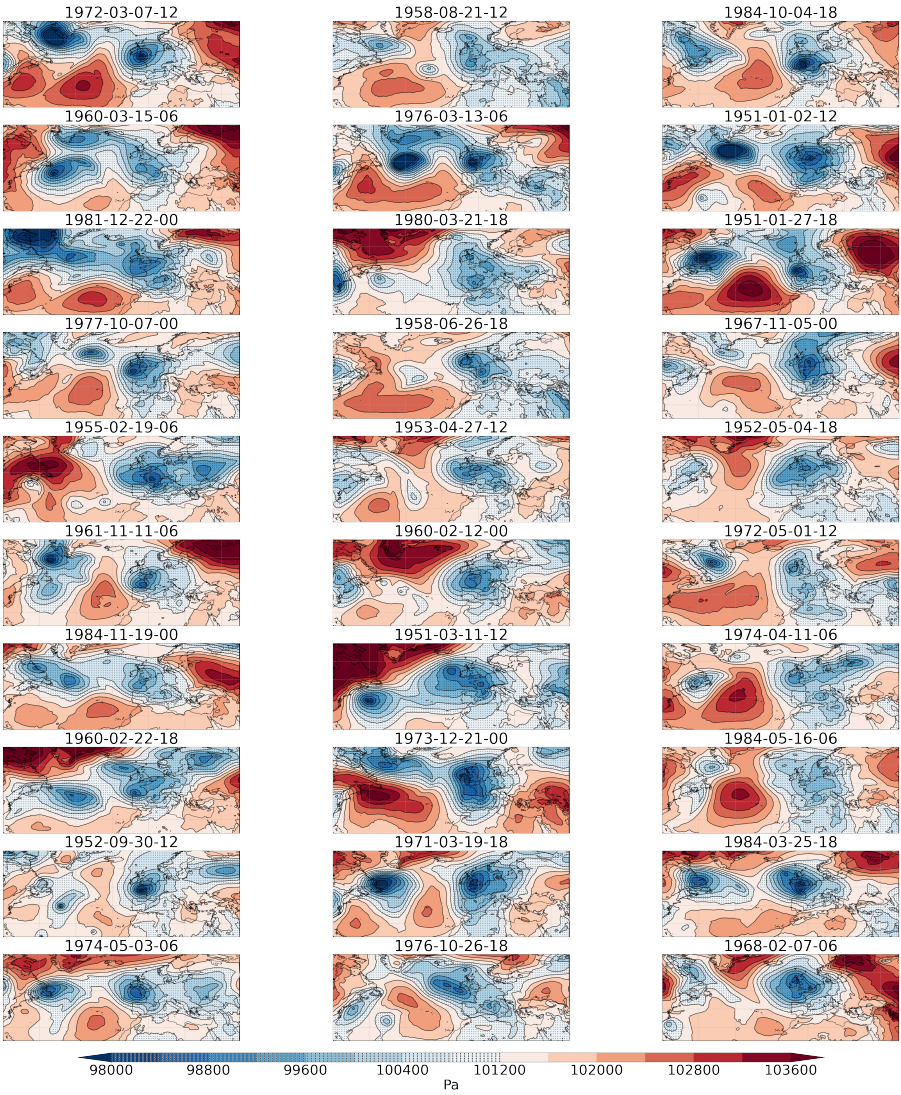

Fig. B3 Mean sea-level pressure of the 30 analogues of cyclone Alex in the counterfactual period.

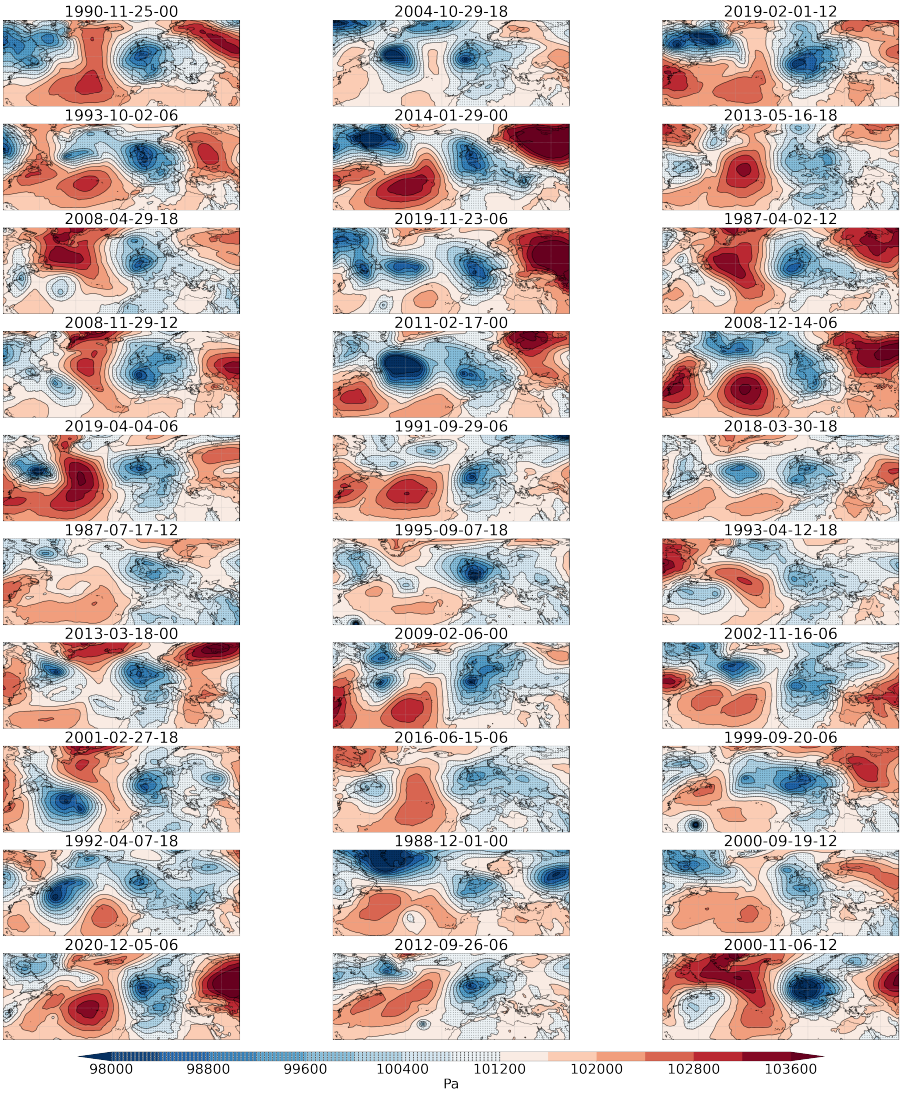

Fig. B4 Mean sea-level pressure of the 30 analogues of cyclone Alex in the factual period.

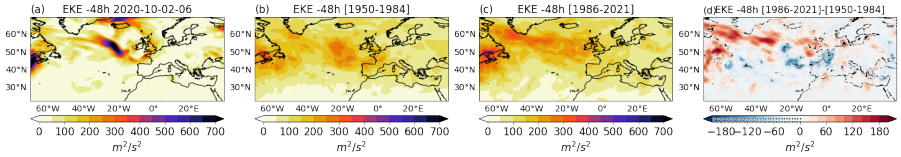

Fig. B5 Same as Fig. 2 (i–l) but for eddy kinetic energy centered 48 hours before Alex's *lag 0* date (a) and analogue *lag 0* dates(b–d).

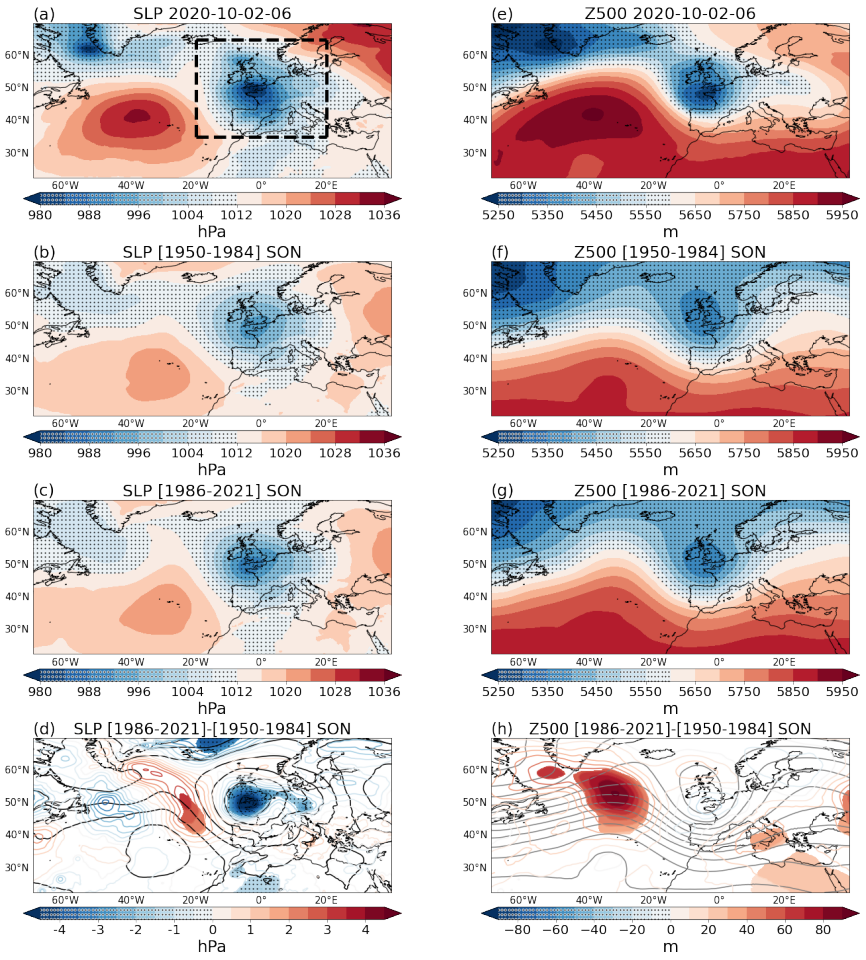

Fig. B6 Same as Fig. 2 (a–h) but for autumn (September-October-November) analogues

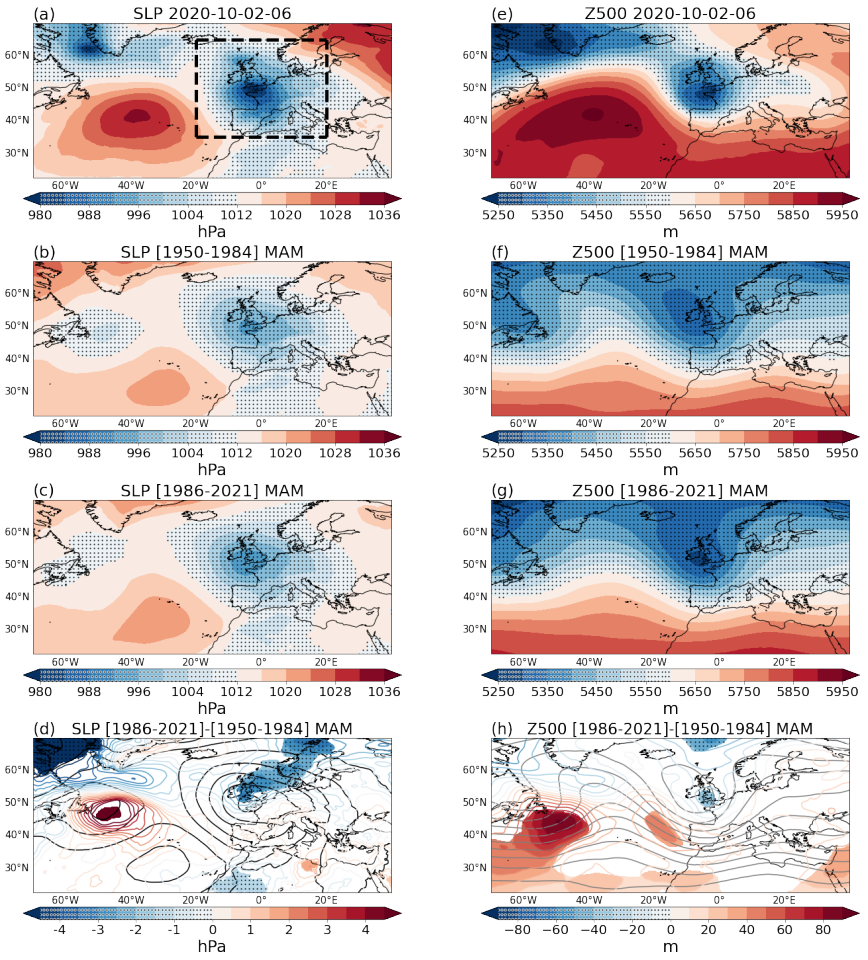

Fig. B7 Same as Fig. 2 (a–h) but for spring (March-April-May) analogues

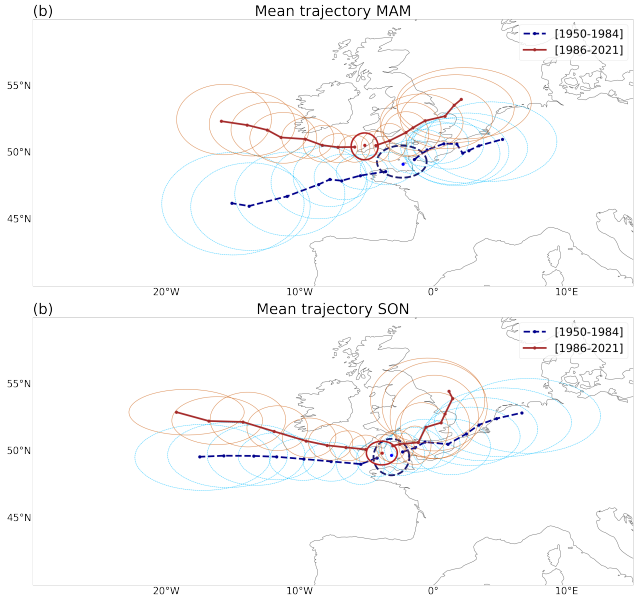

Fig. B8 Same as Fig. 4 but for (a) spring (March-April-May) analogues and (b) autumn (September-October-November) analogues.

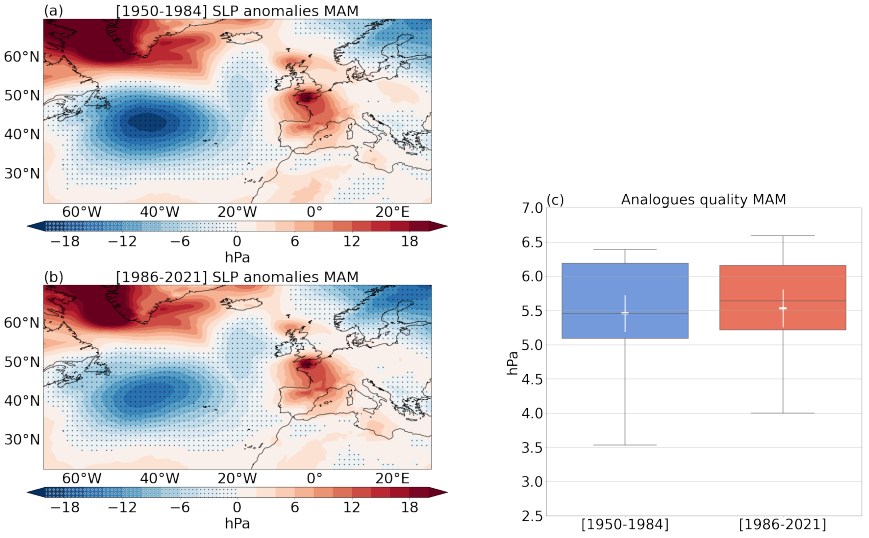

Fig. B9 Same as Fig. 6 but for spring (March-April-May) analogues

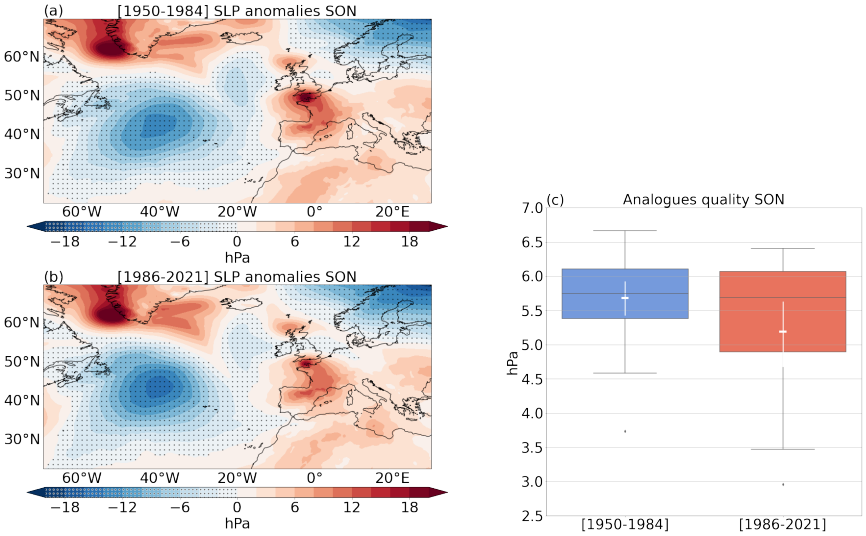

Fig. B10 Same as Fig. 6 (a–h) but for autumn (September-October-November) analogues

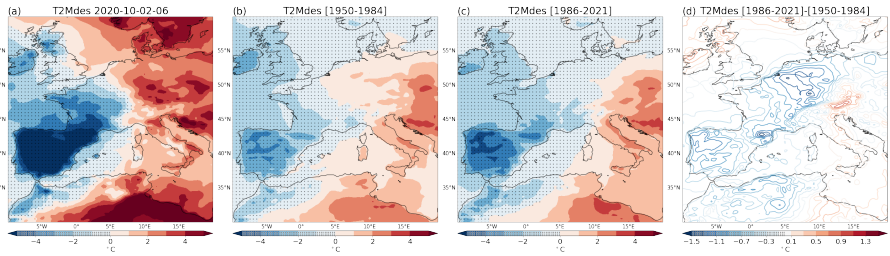

Fig. B11 24-hour means of deseasonalized 2-meter air temperature of Alex (a), counterfactual analogues (b), factual analogues (c) and differences between the analogues in the two periods (d). The start times to compute the temporal mean are the *lag 0* dates and end times are 24 hours after them.

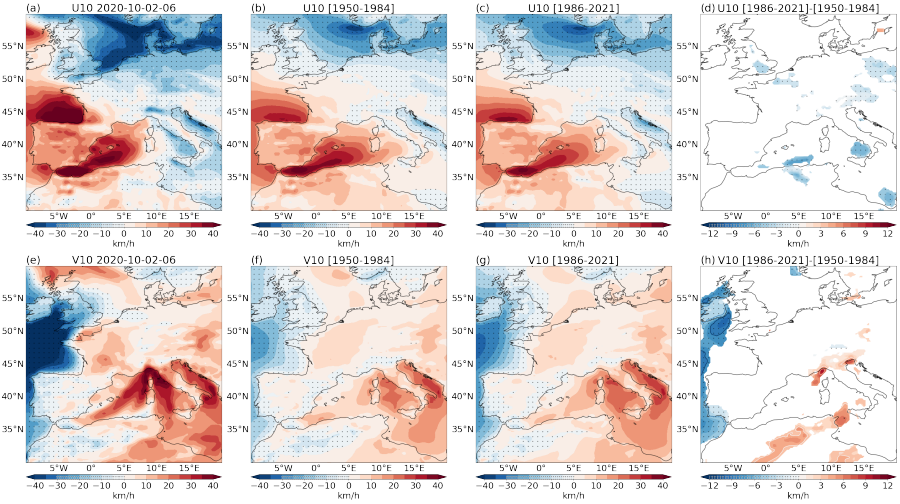

Fig. B12 24-hour means of 10m zonal wind (first row) and 10m meridional wind (second row) for Alex (a, e), counterfactual analogues (b,f), factual analogues (c,g), and difference between the analogues in the two periods (d,h). The start times to compute the temporal means are the *lag 0* dates and end times are 24 hours after them.

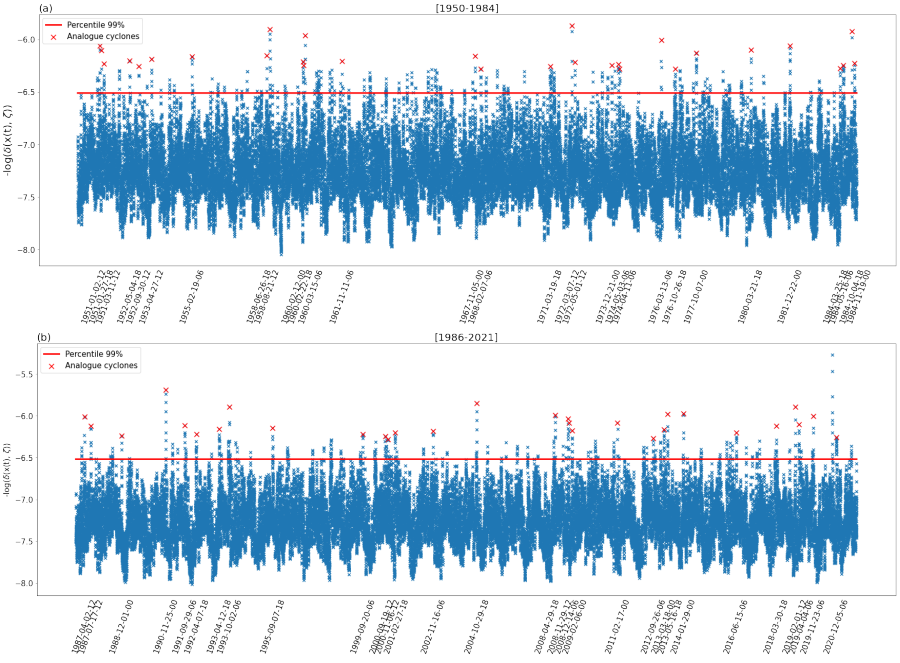

Fig. B13 Timeseries of the $g(x(t))$ distances between Alex and all the other timesteps in the counterfactual (a) and factual (b) periods. Red crosses show the analogue cyclones. *lag 0* dates are indicated on the x-axis. Red lines show the 99% quantile $s(q)$, and the exceedances are used to compute the dynamical system metrics.

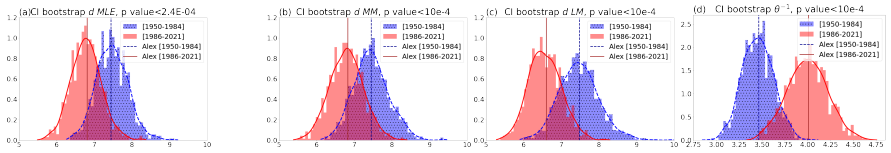

Fig. B14 Boostrap distribution for local dimension d computed using Maximum Likelihood Estimation (a), Method of Moments (b), and L-Moments (c), and for persistence θ^{-1}. The confidence interval is the middle 95% bootstrap distribution. The statistical significance of the difference between factual and counterfactual distributions has been assessed using the Kolmogorov-Smirnov test. P-values are shown in the panel titles, indicating that all the distributions are significantly different at the 5% level.